Built to fight : variable loading conditions and stress distribution in stag beetle jaws

Built to fight: variable loading conditions and stress distribution in stag beetle jaws

Jana Goyens[a,b]*, Joris Dirckx[b] and Peter Aerts[a,c]

[a] University of Antwerp, Laboratory of Functional Morphology, Universiteitsplein 1, B-2610 Antwerpen, Belgium

[b] University of Antwerp, Laboratory of BioPhysics and BioMedical Physics, Groenenborgerlaan 171, B-2020 Antwerpen, Belgium

[c] Department of Movement and Sport Sciences, Ghent University, 9000 Ghent, Belgium

* Corresponding author: +3232652260, jana.goyens@uantwerpen.be

Key words: Lucanidae, Finite Element Modelling, mechanosensor, bite force

Designing very robust structures in an efficient way is a reoccurring challenge in engineering. For male stag beetle weaponry, the solution to this problem was evolved by natural and sexual selection. Stag beetle armature is adapted to perform under extreme circumstances: male stag beetles fight pugnacious battles over females, by using their extremely large jaws as ferocious weapons. During violent encounters, these jaws have to withstand forces with a wide range of unpredictable directions at several application points. We constructed 1020 Finite Element models with different input forces to investigate how the male jaws are structurally adapted to avoid failure. The cross-sectional shape of the jaw is adapted to provide robustness against the reaction forces of biting. Nevertheless, the jaw's shape cannot prevent that bite forces induce relatively high material stresses compared to other force directions. Also, males do not confine themselves in combats to bite with the most robust jaw regions. Both observations emphasise the usefulness of bite force modulation to avoid jaw failure. This is likely effectuated by a sensory network in the jaw exoskeleton, as sensor densities are nicely correlated to the maximal material stress caused by 510 different loading directions. Probably, stag beetles use this sensory information to adjust their fighting strategy as well. Finally, male jaws also need to resist the forceful bites inflicted by opponents. Even though this loading applies at other locations along the jaw, and bends the jaw in the opposite direction, our models show that the jaws are equally robust against these external forces as they are against the forces caused by their own biting.

1. Introduction

A reoccurring challenge in engineering is to design very robust structures in an efficient way. We explore the solution to this problem that was evolved by natural and sexual selection for stag beetle armature. Stag beetle weaponry is adapted to perform under extreme circumstances. Male stag beetle jaws are used in pugnacious fights over females. These jaws are extremely elongated (up to as long as their own body, see Fig. 1) to reach forward to detach the opponent's legs [1]. In an evolutionary arms race, the male head enlarged drastically to house massive bite muscles that enable males to bite seven times as forcefully as females [2]. Hence, their jaws have to be robust enough to withstand high forces; but at the same time, the large and robust jaw structure needs to be as lightweight as possible to minimise the costs of running and flying [3,4]. Consequently, the evolution

of the stag beetle jaw morphology faced a complex trade-off between armature size, robustness and weight.

One answer to this problem is the ability of stag beetles to modulate their bite force very precisely. Throughout the animal kingdom, muscle activity is modulated to fine-tune the produced force and movement. For example, masticatory forces must be adjusted to the material properties of the food in order to prevent tooth damage, and a fine control of finger muscles is vital to enable grasping and prehension [5,6]. With regard to the actuation of animal weapons, an effective muscle force modulation can have a significant fitness impact, as individuals with broken armaments are often excluded from the mating pool [e.g. elk antlers and rhinoceros beetle horns, [7,8]]. Indeed, *Cancer* crabs behaviourally restrain their bite force in function of claw damage [9]. Male *Cyclommatus metallifer* stag beetles even succeed in controlling their bite force precisely enough, in function of the slenderness of the utilised jaw region, to maintain the same material stress [10].This ability probably played a major role in the evolution of stag beetle armature, because it allowed the development of the massive bite muscles (that are necessary to pinch forcefully with the robust mandible parts) while evading the risk to break the slender tips.

Interestingly - especially given the ongoing research for bioinspired strain sensors [11–13] - the stag beetle muscle force modulation is controlled by a system of mechanosensors in the jaws [14]. Previous investigations showed that the distribution of these sensors is highly correlated to the material stress in the jaw during simulated biting at the jaw tips [14]. However, the jaw tip is definitely not the only bite location that male stag beetles use during fights: behavioural observations show that all mandible regions are used to bite, albeit at different frequencies [1]. Moreover, also the direction of the forces acting at the bite point must be very variable. The jaw can be considered a ‘one degree of freedom’ lever, hinging in a single plane as a result of the contraction of the massive jaw adductor ([2] and see Fig. 1 and 2). Nevertheless, the loading of the jaw by the bite-reaction force will only occasionally occur in that plane perpendicular to the jaw hinge while oriented perpendicularly to the jaw lever arm (from now on, we will call this loading ‘pure biting’), because of the shape and texture of the contact surfaces. As a consequence, the reaction forces that the jaw experiences are variable and unpredictable in orientation [15–17]. Further, the jaws are not exclusively utilised to bite, but instead they are used in very various ways during the diverse conducts and behaviours in the battles [1]. The beetles violently wrestle, which causes various forces and torques on the jaws. Sometimes, stag beetles even flip over, with their jaws twisted around the opponents jaw.

Given these various battle conducts and the variable bite-reaction forces, we question how the stag beetle jaw morphology is structurally adapted to withstand the variable force directions on various locations along the jaw shaft. We hypothesise that jaw regions that undergo high stress in any of the force conditions, will possess a high number of sensors. Additionally, we will investigate the influence of the bite force of the opponent (i.e. being bitten) on the jaw stress. This is also very relevant, as these forces can potentially become even higher than the own exerted bite force for a certain bite location. This is, for example, the case when a male is bitten in its jaw tips by the base of the opponent’s jaws, because the jaw base has a short, mechanically advantageous lever and thus a higher bite force than the jaw tip. Also, the jaw bends in another direction, and the material stress of a structure is often different in compression and tension. Furthermore, the beetle cannot control or

modulate the force by which it is bitten. Therefore, we hypothesise that the jaw structure is more robust against forces with directions that are typical for being bitten rather than for those of biting.

We will test our hypotheses using a previously validated Finite Element Model (FE model, [10]). We will calculate the distribution of the material stress under different loading regimes. These loadings will be applied on 5 locations along the jaw shaft, both for biting and being bitten, with a range of force directions. In real battles, some force directions occur more often than others, and we hypothesise that common force directions incur lower material stresses, due to adaptations of the jaw structure. Also the typical force amplitude differs between force directions, and we expect the jaws to be more robust against force directions that are associated with high amplitudes. Therefore, we will simulate all force directions at the same amplitude, to compare whether force directions that have a low amplitude in reality induce higher material stresses than force directions that typically have a high amplitude. Finally, we will compare the material stress distribution of the 1020 FE models between loading conditions and with the sensor distribution that was deduced from micro CT scans and Scanning Electron Microscopy.

2. Material and methods

We developed an FE model of a jaw of an adult male *Cyclommatus metallifer* stag beetle in the FEBio software suite (FEBio 1.4.1, [18]). This species was chosen for its large armature and its eagerness to engage in combats [1]. The male jaw has an elongated, slightly curved shape with several teeth and serrations (see Fig. 1). There is a ridge in the medial jaw surface over the entire length of the jaw. At the proximal half, there is also a dorsal and a ventral ridge in the lateral jaw surface, which results in a triangular cross-section (see Fig. 1). The bite muscle attaches to the jaw at the medial side of its base. The rotation hinge is located at the lateral side of the base (see Fig. 2).

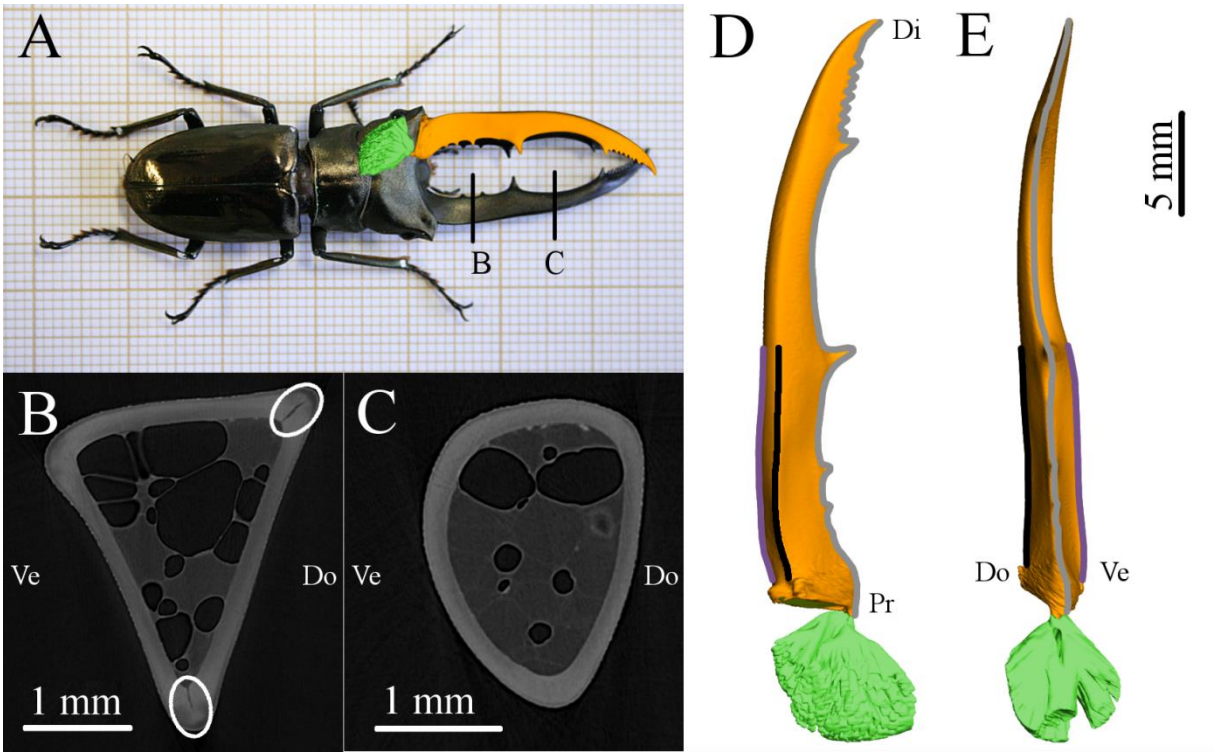

Figure 1 Jaw morphology. A: Photo of a male *Cyclommatus metallifer* stag beetle. A 3D model of one jaw and its bite muscle are superimposed on the picture. The location of the cross-sections in panels B and C are

indicated with vertical lines. B and C: Transverse micro CT slice in respectively the proximal and distal jaw half. The location of 2 dendrite channels, which lead to a mechanosensor at the jaw surface, are encircled. D and E: 3D model of a male jaw (orange) and its bite muscle (green) in respectively dorso-lateral and medial view. The medial (inner) jaw ridge is indicated in grey, the dorsal lateral ridge in black and the ventral lateral ridge in purple. The proximal (Pr), distal (Di), dorsal (Do) and ventral (Ve) sides of the jaw are designated

For the construction, material properties and experimental validation of the FE model, we refer to [10]. The jaw geometry was inferred from a micro CT scan (Skyscan 1172, Bruker, Kontich Belgium; see Fig. 1B,C), which was operated at a voltage of 70 kV, a current of 141 µA, an exposure time of 440 ms and a rotation angle of 0.2°. The 3D volume of the jaw cuticle was determined in the 3D image processing software Amira (Amira 5.4.4; 64-bit version, FEI, Hillsboro, OR, USA). This was converted in a tetrahedral volume mesh with TetGen software [19]. The jaw cuticle was modelled as an isotropic and linear elastic material. Double Indentation experiments indicated that its Young's modulus is 5.1 ± 1.3 GPa. Because the Poisson ratio of insect cuticle is, to the best of our knowledge, not known in literature, and because the Poisson ratio had only negligible effects on the model behaviour, we used an intermediate value of 0.3. The movement (translation and rotation) of the muscle attachment region of the jaw was constrained, representing an isometric muscle contraction. The jaw model rotated about its joint axis (see Fig. 2). In each model, a different force was exerted at the medial ridge of the jaw. We chose 5 force application positions, based on behavioural observations [1]. From proximal to distal, the forces were applied at the positions 'Near' (N), 'Protrusion' (*P*), 'Far' (*F*), 'Tip Tooth' (*TT*) and 'Tip' (*T*) (see Fig. 2, one application zone per FE model). The forces were applied to a small group of FE elements at these positions (an application 'zone'), and there was only one application zone for each FE model. The force magnitudes at the application zones *P* and *T* were those that were measured in bite force experiments [10], and these were used to deduce the force magnitudes in the other zones (taking the length of the lever arm linearly into account, see Table 1). For each zone, 102 force vectors with the same amplitude but with a different direction (orientation) were sequentially implemented in the FE model (see Fig. 2). The direction of these vectors ranged from the reaction force of pure biting (*b* on Fig. 2, force vector perpendicular to lever arm and joint axis; cf. above) to compression & tension (*c* & *t* on Fig. 2, force vector aligned with lever arm) and upward & downward bending (*u* & *d* on Fig. 2, force vectors aligned with jaw joint axis). Pure bite forces (*b*) will cause the jaw to bend in the frontal plane (the xy-plane, see Fig. 2A), while upward and downward forces (*u* & *d*) will cause bending in the sagittal plane (the yz-plane, see Fig. 2A). Because of the irregular jaw shape, the so-called compressive and tensile forces (*c* & *t*) will not only compress or stretch the jaw, but they will also bend it. The 3D direction of the 102 force vectors was determined with the 'ParticleSampleSphere' function in Matlab (Matlab R2013b, 64 bit version, Natick, Massachusetts), to have an even distribution on a hemisphere. We used a hemisphere of force directions, rather than a complete sphere, as a reaction force that pulls on the jaw is highly unlikely in the context of stag beetle fights.

On a symmetrical structure, forces of the same magnitude but opposite sense will result in the same deformations and stresses. On an asymmetrical structure, this is not the case. As this may seem surprising at first glance, we show an example in figure 3. A part of a toroid with a square cross section is used as a highly simplified model of the curved beetle jaw (radius: 27 mm; width and height: 3 mm). The base of the structure is fixed, and the tip is loaded with forces along three orthogonal directions. For forces in opposite directions along the X-axis (*b* and *-b*) the maximal stress differs by 17%. For forces along the Y-direction (*c* and *t*), the difference is 12%. These differences are

caused by the geometrical asymmetry of the model. For the symmetrical direction of the model (forces aligned with the Z-axis, *u* and *d*), the maximal stress is identical.

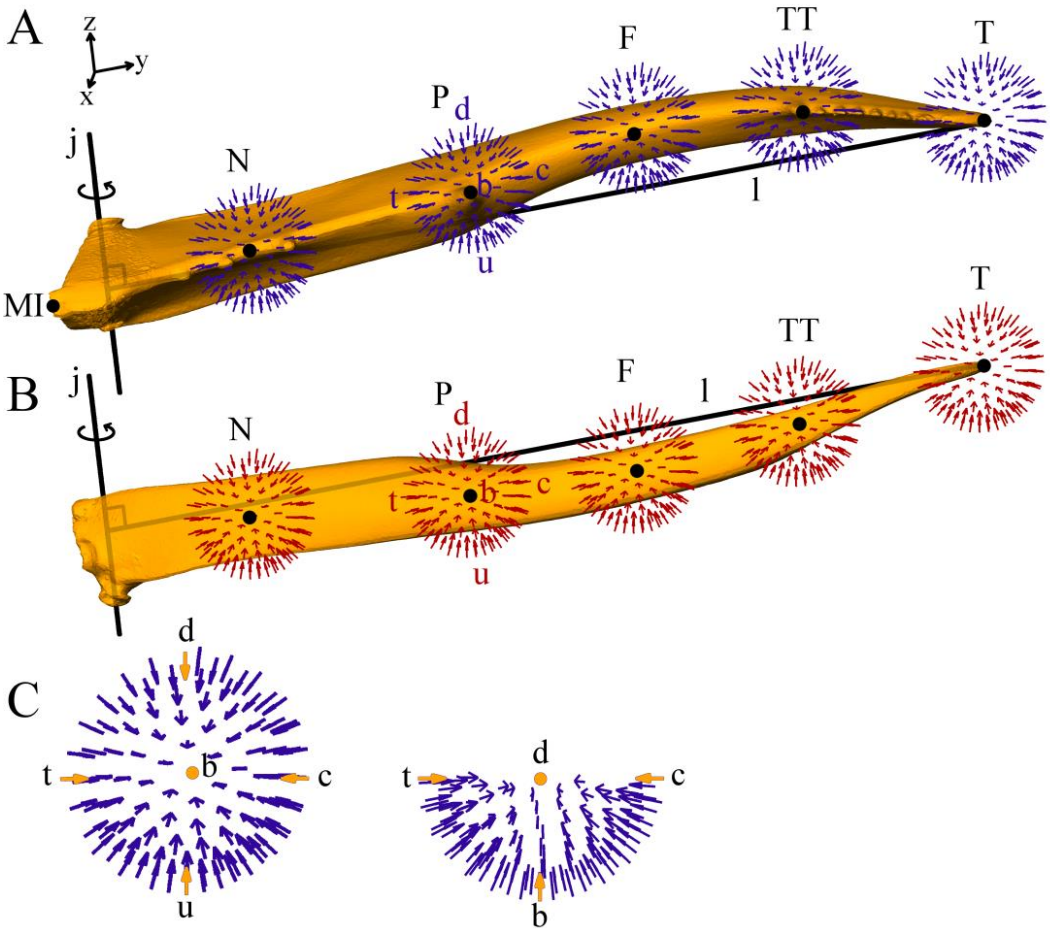

Figure 2 Overview of the FE models. A and B: 3D model of the stag beetle jaw (orange), respectively in medial and lateral view. The application zones *N*, *P*, *F*, *TT* and *T* are indicated (black dots), as well as the joint axis (j) and the lever arm (l) of application zone *T*. The force directions down (*d*), up (*u*), tension (*t*), compression (*c*) and biting (*b*) are designated for application zone *P*. The muscle attachment region is fixed (*MI* in A). The 102 force vectors per application zone are depicted in purple (A) or red (B). The coordinate system is depicted for A. C: Enlargement of the force directions in medial (left) and dorsal (right) view

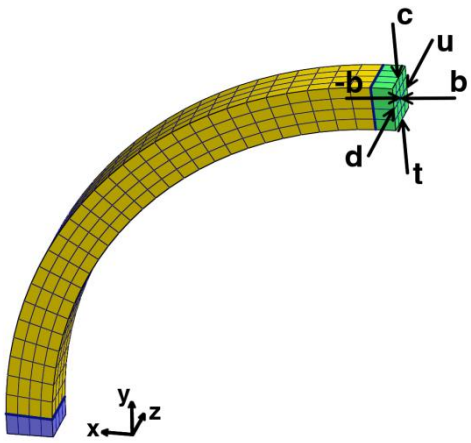

Figure 3 Model of a simple, curved structure (part of a toroid with a square cross section). The base is constrained, and a force is applied to the tip.

To simulate the jaw deformations when a jaw is bitten by an opponent, we used the same force applications zones, yet transposed to the contralateral side (the lateral side) of the jaw (see Fig. 2B). The hemisphere of force directions was mirrored in the plane of the lever arm and the joint axis, so that the force vectors were pushing into the mandible (not pulling).

For all models, each with a different input force on the jaw, we calculated the maximal Von Mises stress and the Von Mises stress distribution in the jaw with FE routines, and exported these to Matlab. We compared these model outcomes with the mechanosensor distribution in the same jaw. For a detailed description of the sensor anatomy, we refer to [14]. Scanning and Transmission Electron Microscopy (SEM and TEM) revealed that the jaws contain a high number of small mechanosensors. The sensors have a small bristle that stimulates the dendrite tip when the jaw is deformed (see Fig. 4, obtained by a Quanta 250 FEG microscope, FEI, Hillsboro, OR, USA; [14]). The number of sensors in 28 square patches of 1 mm^2 were manually determined on a micro CT scan in the 3D image processing software Amira (Amira 5.4.4; 64-bit version, FEI, Hillsboro, OR, USA, see Fig. 1B). On the micro CT scans, the dendrite channels were clearly visible. Because each channel leads to one bristle at the outer jaw surface, both have an identical distribution. We also determined the sensor density in 4 additional patches on the dorsal and ventral lateral ridges (for an overview of all patches, see Fig. 5). Next, we compared the sensor distribution with the material stresses that are caused by a large range of force directions (in all 32 patches).

Table 1 Force magnitude and lever arm for each force application zone

Zone	Force	Lever arm
N	4.4 N	4.2 mm
P	3.4 N	11 mm
F	2.7 N	16 mm
TT	1.9 N	21 mm
T	1.2 N	27 mm

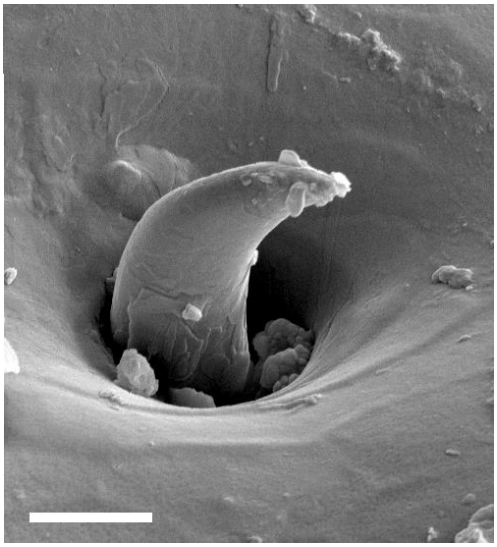

Figure 4 SEM photo of the external part of a mechanosensor on a stag beetle jaw. The scale bar indicates 5 µm. The microscope was operated at a voltage of 10 kV.

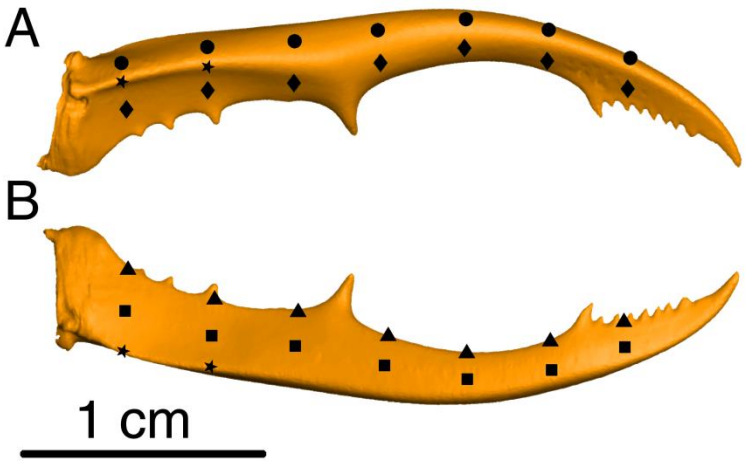

Figure 5 Location of 32 square patches of 1 mm² that were used to count the sensors on a 3D model of a male jaw. A: Ventral lateral view, with indication of the patches on the lateral jaw surface (circles), ventral lateral ridge (stars) and the ventral jaw surface (diamonds). B: Dorsal view, with indication of the patches on the medial ridge (triangles), dorsal jaw surface (squares) and the dorsal lateral ridge (stars)

3. RESULTS

3.1 Influence of force direction on material stress

Stress distribution

When the direction of the input force changes, the stress distribution in the jaw, as well as its maximal value, varies (see Fig. 6). Even though the maximal stress amplitude fluctuates gradually as the force direction changes, the location of this stress maximum is not always the same (see Fig. 6). The highest stress is not always located in the close proximity of the application zone either. For application zones *TT*, *F* and *P*, upward and downward bending (*u* & *d*) most often cause elevated stress on both lateral ridges on the proximal jaw part, while bending in the frontal plane (caused by force direction *b*) raises the material stress in the proximal part of the medial ridge (see Fig. 5). The same is true for forces on the very tip of the jaw (*T*), yet the maximal material stress is found very distally along the jaw. For all application zones, opposite forces (*u* versus *d*; *c* versus *t*) cause very similar stress distribution patterns.

Maximal stress amplitude

For all application zones, the maximal amplitude of the material stress fluctuates gradually as the force direction changes, with minima for pure compression and tension (see Fig. 6). The pattern of stress fluctuation does however differ between application zones. For the application zone at the very tip of the jaw (*T*), the highest material stress is caused by forces that combine directions *b*, *u* and *t* (frontal and upward bending and stretching). The stress amplitude is higher than for any other application zone (up to 96 MPa). The maximal amplitude of the Von Mises stress in the more proximal zones *TT*, *F* and P are respectively 71 MPa, 78 MPa and 62 MPa (see Table 2). The fluctuation patterns of the maximal stress amplitudes on the hemisphere are highly comparable for these three application zones, with a maximum close to force direction *b* (pure biting). There is also a second group of force directions with elevated stress, for pure downward bending for application zones *TT* and *F*. For the most proximal application zone (*N*), the maximal Von Mises stress is always very low and the highest Von Mises stresses (up to only 35 MPa) are found for pure upward or downward bending.

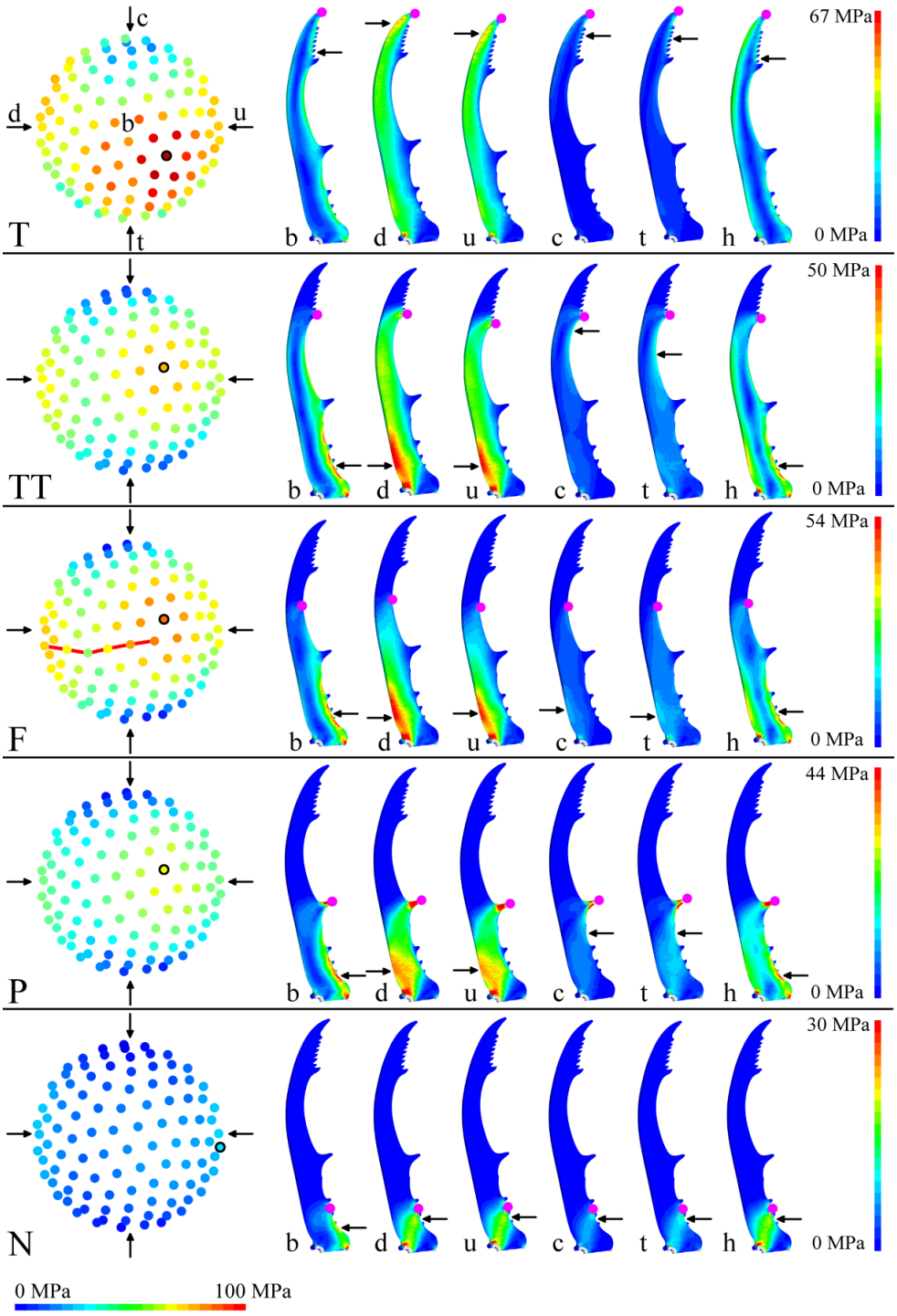

Figure 6 Maximal Von Mises stress per application zone (*T*, *TT*, *F*, *P* and *N*) for all force directions (left, scale bar in left bottom corner) and Von Mises stress distributions for 6 selected force directions (right, scale bars at right border). The maximal Von Mises stresses are represented by coloured dots on a top view of the hemisphere of force directions (medial view on jaw). The force direction that elicits the highest stress (*h*) is marked with a black circle. For application zone *F*, force directions ranging from downward bending (*d*) to pure biting (*b*) are connected with a red line. Arrows indicate the direction of downward (*d*) and upward (*u*) bending, compression (*c*) and tension (*t*). For force directions *b*, *d*, *u*, *c*, *t* and *h*, a dorsal view of the stress distribution on the jaw is depicted on the right. Pink dots locate the application zone and arrows indicate the jaw region with the highest stress

3.2 Sensor distribution

The proximal half of the jaw has a triangular cross-sectional shape. The vertices of these triangles (the jaw ridges) experience high material stresses, because they are furthest from the neutral bending axis. As a consequence, the location of high stress does not move gradually from ridge to ridge when the force direction gradually changes (see Fig. 7). Instead, the elevated material stress disappears at one ridge and reappears at another. This corresponds to the sensor distribution, which has a very high sensor density in the ridges, and a low density on the flat surfaces in between.

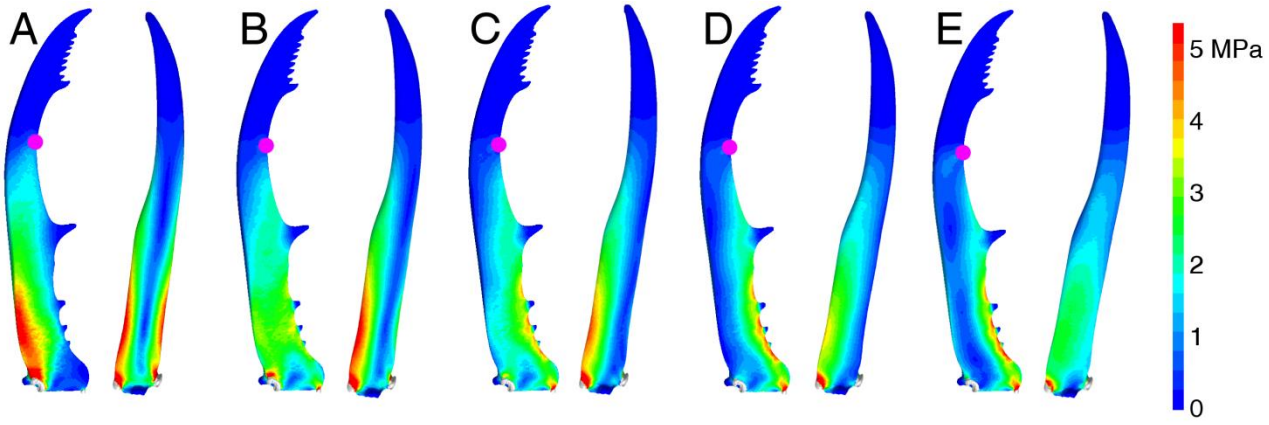

Figure 7 FEM models of application zone F, with force directions ranging from downward bending (A) to bending in the frontal plane (E; the transect is indicated in Fig. 6, application zone F). Figure panels B to D represent force directions in between those of A and E. The distribution of the Von Mises stress is shown in dorsal view (left) and lateral view (right). Pink dots locate the application zone

Figure 8 shows the relationship between the number of sensors and the material stress that is experienced by the same jaw region (patch) due to any of the force directions. There is weak positive relationship between both, which is strongest for bending in the frontal plane (i.e. caused by pure biting). For all force directions, the correlation is reduced by data points with a low material stress at locations with a high number of sensors. For example, the lateral ridges (stars in Fig. 5) experience low material stress by pure biting (up to about 30 MPa), but undergo high stress by upward and downward force directions (up to about 60 MPa). However, the number of sensors only needs to be adapted to the highest stress at that location. Hence, if we only retain the highest material stress for each jaw region, we find a relatively high correlation coefficient (0.69, see Fig. 9).

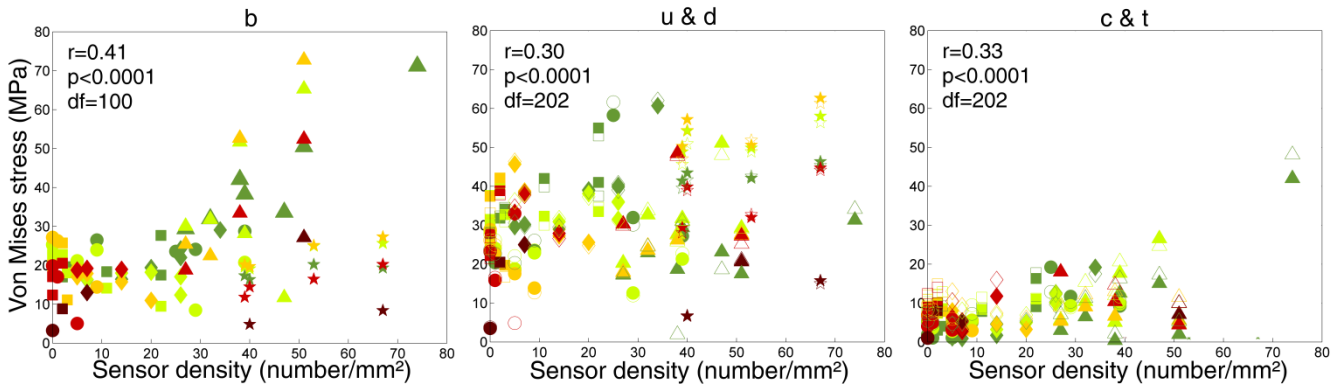

Figure 8 Relation between number of sensors and Von Mises stress. Results are shown for the force directions *b*, *u*&*d* and *c*&*t*. Marker shape indicates different jaw regions: dorsal (squares), ventral (diamonds), lateral (circles) and medial side (triangles) and the dorsal and ventral lateral ridges (stars). Marker colour indicates the application zone: dark green (*T*), light green (*TT*), yellow (*F*), red (*P*) and brown (*N*). Filled symbols are used for the force directions *b*, *u* and *c*; hollow symbols for *d* and *t*

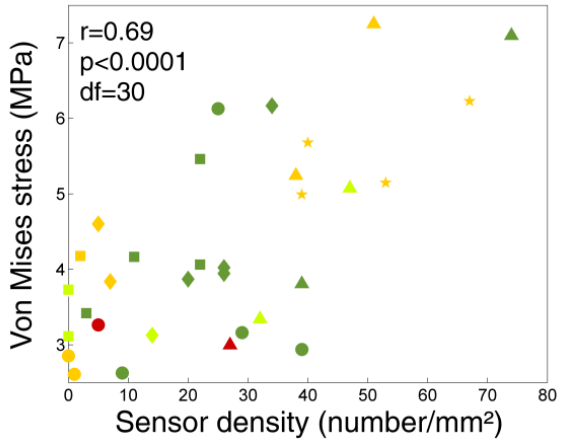

Figure 9 Correlation between the sensor density and Von Mises stress. Only the force directions that cause the highest stress in a certain jaw region are shown. Marker shape indicates different jaw regions: dorsal (squares), ventral (diamonds), lateral (circles) and medial side (triangles) and the dorsal and ventral lateral ridges (stars). Marker colour indicates the application zone: dark green (T), light green (TT), yellow (F), red (P) and brown (N).

3.3 Biting versus being bitten

Except for application zone T, the effect of the force direction on the maximal stress is largely similar between biting and being bitten (see Fig. 6 and 10). The act of biting causes more material stress in the jaws than being bitten by the same force amplitude (two-way anova: $p_{biting/beingbitten}=0.001$, $p_{applicationzone}=0$, $p_{interaction}=0.014$; see Table 2). This difference is relatively large for application zones *T*, *P* and *N* (up to 26%), but small or non-existent for application zones *TT* and *F* (see Table 2). The observed differences can be attributed to both geometrical asymmetry and differences in the lever arm length and the angle between the lever arm and the force vectors (especially for the more proximal application zones).

Table 2 Von Mises stress when biting and being bitten, and the relative difference between both. The stress maximum, mean and standard deviation are given for each application zone separately (*T*, *TT*, *F*, *P* and *N*) and for all zones together

Application	**Biting**		**Being bitten**		**% difference**	
zone	Max	Mean ± SD	Max	Mean ± SD	Max	Mean
T	96	62 ± 15	88	56 ± 15	-8.3%	-9.7%
TT	71	49 ± 14	68	49 ± 14	-4.2%	0%
F	78	53 ± 16	76	54 ± 16	-2.6%	1.9%
P	62	41 ± 12	54	37 ± 10	-13%	-9.8%
N	35	24 ± 5.7	26	19 ±4.4	-26%	-21%
all	96	46 ± 18	88	43 ± 19	-8.3%	-6.5%

4. Discussion

Male stag beetle jaws have to withstand a wide variety of forces when they are utilised as weaponry in male-male battles. We aimed to understand how the jaw morphology is adapted to resist deformations caused by these forces. Concomitantly, we investigated the relationship between the material stress and the density of the sensors that may be used to modulate the jaw deformations.

4.1 Maximal stress distribution and amplitude

We hypothesised that the structure of the stag beetle jaw would be adapted to withstand those force directions that are common in battle situations and that typically have a high magnitude. Due to their large bite muscles, the highest loads on the jaws are probably caused by biting (they bite up to 3 times as forceful as the female bite, even after size-normalisation [2]). We indeed observe structural adaptations against 'pure biting' forces. The distal jaw region (near application zone *F*) has an elliptical cross-section (see Fig. 1), with the long axis along the force direction *b*. Therefore, it is more robust to withstand bending in the frontal plane than would be with a circular cross-section. A similar adaptation has been observed in *Dynastes hercules* rhinoceros beetles [20]. This bending resistance not only protects the stag beetle jaw against failure, but also guarantees a firm grip on the opponent. However, a negative side effect of the elliptical cross-section is that it makes the jaw more sensitive to bending in the sagittal plane (force directions *u* and *d*). The jaw base is even more bending resistant than the distal jaw region, due to its triangular cross-section (see Fig. 1). A triangular cross-section has more material further from the neutral axis to resist the high material stress at these locations (in a lot of our FE simulations, the material stress in the jaw ridges is indeed very high, see Fig. 6). The high bending resistance of the jaw base is very useful in the male fighting strategy, because the grip on the opponent would be lost if the jaw base bent. This reasoning also holds true for bites at the distal jaw regions.

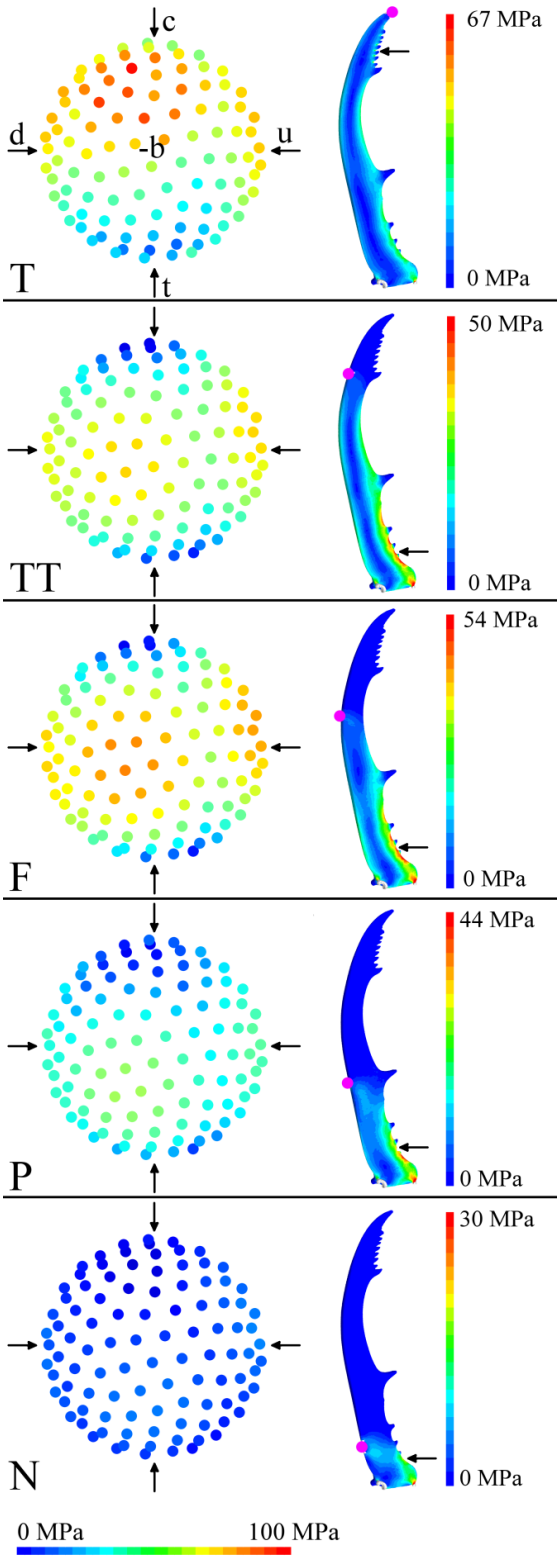

Figure 10 Left: maximal Von Mises stress per application zone (*T*, *TT*, *F*, *P* and *N*) for all force directions (scale bar in left bottom corner). These maxima are represented by coloured dots on a top view of the hemisphere of force directions (medial view on jaw). Arrows indicate the direction of downward (*d*) and upward (*u*) bending, compression (*c*) and tension (*t*). Right: Von Mises stress distributions for bending in the frontal plane (force direction *–b* , scale bars at right border). Pink dotes locate the application zone and arrows indicate the jaw region with the highest stress

The material stress in the male stag beetle jaw depends strongly on the direction of the force acting upon it (see Fig. 6). Despite the adaptations of the cross-sectional shape to resist 'pure' bite forces, our FE analyses show that they induce high material stresses, compared to other force directions (see Fig. 6). Even though the upward and downward forces (*u* & *d*) in stag beetle fights are a lot lower than the bite force, the jaws are more robust against them (except for application zone N). Probably, this is a side-effect of the triangular jaw base. Compared to force directions *u* and *d*, pure biting possibly causes more stress due to the notches between the protrusions (large and small teeth) on the medial jaw ridge. For application zone N, force directions *u* and *d* cause more material stress than pure biting, and their location of maximal stress is also located between two protrusions at the medial ridge. For all application zones, the lowest material stress is produced by force directions *c* and *t*. These forces cause relatively more compression and tension, and less shear, which results in a lower material stress. This robustness is convenient for the losing male stag beetle when it falls on the tips of its jaws after being lifted and thrown by its opponent [1]. The impact forces increase quickly with the distance fallen. For example, when a beetle (mass of 2 g) falls down from a tree log onto the ground (e.g. 20 cm), the impact force is already 3.9 N (assuming that its jaw tips penetrate the substrate for 1 mm). This rough force estimation largely exceeds the maximal tip bite force (1.2 N, see Table 1). In reality, stag beetles may often fall from much higher distances, given their eagerness to climb on tree trunks and branches [21]. However, falls on the tips may not happen very frequently, and therefore, the accompanying low material stress may rather be an lucky coincidence than an adaptation.

The highest Von Mises stresses are observed for forces at the very tip of the mandible (application zone *T*, up to 96 MPa). Nevertheless, battle observations showed that stag beetles do use this application zone in ±10% of the bites [1]. Moreover, application zone F, which is the most frequently used biting zone (±30% of the bites, [1]), causes the second highest Von Mises stresses (up to 78 MPa). Hence, they frequently use their bite force modulation mechanism to reduce the fracture risk in real fight situations [10]. Due to the modulation of the bite force for tip biting, they increase the safety factor from 4.3 to 5.2, and as a result, the material stress does not increase above the stress that is induced by the real bite force at application zone P [10].

4.2 Sensor distribution

The sensor density on the stag beetle jaws depends on the maximal stress that a jaw region experiences (see Fig. 6,7,9). This is not always the stress that is caused by biting (*b*). For example, the bite force direction causes hardly any stress in the lateral ridges. Hence, the high number of sensors in the lateral ridges can be attributed to upward and downward bending forces (*u* & *d*). Therefore, through evolution, the jaws probably also had to be adapted to withstand other force directions than pure biting.

Further, the mechanosensors may not only be used in a negative feedback mechanism to prevent jaw damage, but they may also be used to assess their opponent and to optimise their fighting strategy. Also other insects control their movements with sensors: male *Trypoxylus dichotomus* beetles use their horns to estimate their opponent's size, flies adapt their flight direction according to the relative position of their halteres to their body, and the walking patterns of cockroaches are controlled with deformation sensors on their tibia [22–24]. If the stag beetle jaws indeed have a sensory role, the slenderness of their tips may have a second function, besides weight reduction [10,14]. A slender jaw tip deforms more rapidly, and may, therefore, provide more precise

information about the opponent's strength and the course of the battle. This may be particularly useful for stag beetles, as they do not always rely on visual information during fights [1]. It would be interesting to test whether they primarily use their jaw tips in the early stages of battles. This would indicate that they mainly use their jaw tips to estimate their opponent's strength, rather than to monitor the course of the battle or to dislodge it from the substrate.

4.3 Biting versus being bitten

We hypothesised that the jaw would be more robust against forces that are typical for being bitten by an opponent, rather than against those typical when biting. The logic behind the hypothesis is that a beetle cannot control or modulate the opponent's bite force, and moreover that its slender distal jaw region may be subject to the high bite forces of the jaw base of the opponent. When taking all application zones into account, the material stress is indeed higher for biting than for being bitten, but the difference is rather small. Further, this difference is not present for application zones *F* and *TT*, even though they are more prone to material stress than application zones *P* and *N* (especially because these distal jaw regions can be bitten by the jaw base of their opponent). Hence, we conclude that the stag beetle jaw structure is not especially adapted to withstand the bite forces of their rivals.

In reality, the direction of the forces that apply on the jaw when it is bitten by a rival, is probably less variable than for biting. For example, they will never compress or stretch the jaw. Nevertheless, we see no specific adaptations regarding the force direction either: the influence of the force direction on the maximal material stress is very similar to that of biting.

5. Conclusion

Our Finite Element models of male stag beetle jaws indicate a strong influence of the force direction on material stress amplitude and distribution. We found that the jaw structure is not specifically adapted to withstand being bitten, even though the beetles cannot control these forces. The elliptical distal cross-section and the triangular proximal cross-section provide jaw robustness against own bite forces. But even with these structural adaptations, force directions that only slightly deviate from pure biting (force direction *b*) cause the highest material stresses. The beetles overcome this vulnerability by modulating their bite force with a network of deformation sensors. The distribution of this sensory network is adapted for several force directions. Due to the slender jaw tips, these sensors may also be used to control the fighting strategy, by providing information on the opponent's strength and the course of the battle.

Acknowledgements

The present study was funded by a BOF grand [ID BOF UA 2011-445-a] of the Research Council of University of Antwerp. The SkyScan 1172 high resolution micro CT scanner, located at the VUB facilities, was funded by the Hercules Foundation of the Flemish Government [grant UABR/11/004]. The authors thank Mr. Nicolaas Lousberg, Mr. Stijn Van den Broeck and Prof. Sara Bals of the Electron Microscopy for Material Science group at the University of Antwerp for the SEM (partly funded by the Hercules foundation of the Flemish Government). The authors thank Professor Gunther Steenackers for feedback on the mechanical theory behind this study and Ms Josie Meaney for proofreading the manuscript.

6. References

1. Goyens, J., Dirckx, J. & Aerts, P. 2015 Stag beetle battle behaviour and its associated anatomical adaptations. *J. Insect Behav.* **28**, 227–244. (doi:10.1007/s10905-015-9495-3)

2. Goyens, J., Dirckx, J., Dierick, M., Van Hoorebeke, L. & Aerts, P. 2014 Biomechanical determinants of bite force dimorphism in Cyclommatus metallifer stag beetles. *J. Exp. Biol.* **217**, 1065–1071. (doi:10.1242/jeb.091744)

3. Goyens, J., Dirckx, J. & Aerts, P. 2015 Costly sexual dimorphism in Cyclommatus metallifer stag beetles. *Funct. Ecol.* **29**, 35–43. (doi:10.1111/1365-2435.12294)

4. Goyens, J., Van Wassenbergh, S., Dirckx, J. & Aerts, P. 2015 Cost of Flight and the Evolution of Stag Beetle Weaponry. *J. R. Soc. Interface* **12**, 20150222.

5. Crago, P. E., Peckham, P. H. & Thrope, G. B. 1980 Modulation of muscle force by recruitment during intramuscular stimulation. *IEEE Trans. Biomed. Eng.* **27**, 679–84. (doi:10.1109/TBME.1980.326592)

6. Ross, C. F., Dharia, R., Herring, S. W., Hylander, W. L., Liu, Z.-J., Rafferty, K. L., Ravosa, M. J. & Williams, S. H. 2007 Modulation of mandibular loading and bite force in mammals during mastication. *J. Exp. Biol.* **210**, 1046–63. (doi:10.1242/jeb.02733)

7. McCullough, E. L. 2014 Mechanical limits to maximum weapon size in a giant rhinoceros beetle. *Proc. R. Soc. B* **281**, 20140696. (doi:10.1098/rspb.2014.0696)

8. Johnson, H. E., Bleich, V. C. & Krausman, P. R. 2005 Antler Breakage in Tule Elk, Owens Valley, California. *J. Wildl. Manage.* **69**, 1747–1752. (doi:10.2193/0022-541X(2005)69[1747:ABITEO]2.0.CO;2)

9. Taylor, G. 2000 Variation in safety factors of claws within and among six species of Cancer crabs (Decapoda: Brachyura). *Biol. J. Linn. Soc.* **70**, 37–62. (doi:10.1006/bijl.1999.0385)

10. Goyens, J., Soons, J., Aerts, P. & Dirckx, J. 2014 Finite Element modelling reveals force modulation of jaw adductors in stag beetles. *J. R. Soc. Interface* **11**, 20140908. (doi:10.1098/rsif.2014.0908)

11. Skordos, a, Chan, P. H., Vincent, J. F. V & Jeronimidis, G. 2002 A novel strain sensor based on the campaniform sensillum of insects. *Philos. Trans. A* **360**, 239–53. (doi:10.1098/rsta.2001.0929)

12. Menon, C., Brodie, R., Clift, S. & Vincent, J. F. V. 2009 Concept design of strain sensors inspired by campaniform sensilla. *Acta Astronaut.* **64**, 176–182. (doi:10.1016/j.actaastro.2008.07.007)

13. Wicaksono, D. H. B., Vincent, J. F. V, Pandraud, G., Craciun, G. & French, P. J. 2005 Biomimetic strain-sensing microstructure for improved strain sensor: fabrication results and optical characterization. *J. Micromechanics Microengineering* **15**, S72–S81. (doi:10.1088/0960-1317/15/7/011)

14. Goyens, J., Dirckx, J. & Aerts, P. 2015 Mechanoreceptor distribution in stag beetle jaws corresponds to the material stress in fights. *Arthropod Struct. Dev.* **44**, 201–208. (doi:10.1016/j.asd.2015.03.003)

15. Cleuren, J., Aerts, P. & De Vree, F. 1995 Bite and joint force analysis in Caiman crocodilus. *Belgian J. Zool.* **125**, 79–94.

16. Herrel, a., Aerts, P. & Vree, D. 1998 Static biting in lizards: functional morphology of the temporal ligaments. *J. Zool.* **244**, 135–143. (doi:10.1111/j.1469-7998.1998.tb00015.x)

17. Herrel, A., Aerts, P. & Vree, F. D. E. 1998 Ecomorphology of the Lizard Feeding Apparatus: a Modelling Approach. *Netherlands J. Zool.* **48**, 1–25.

18. Maas, S. a, Ellis, B. J., Ateshian, G. a & Weiss, J. a 2012 FEBio: Finite Elements for Biomechanics. *J. Biomech. Eng.* **134**, 011005. (doi:10.1115/1.4005694)

19. Si, H. 2015 TetGen, a Quality Tetrahedral Mesh Generator. *AMC Trans. Math. Softw.* **41**, 11.

20. McCullough, E. L., Tobalske, B. W. & Emlen, D. J. 2014 Structural adaptations to diverse fighting styles in sexually selected weapons. *Proc. Natl. Acad. Sci.* **2014**, 1–5. (doi:10.1073/pnas.1409585111)

21. Suzuki, T. 1996 Some ecological notes of Cyclommatus metallifer metallifer in Sulawesi, Indonesia - Adult feeding habits and possibility of guarding behavior on stag beetles. *Gekkan-Mushi* **305**, 16–19.

22. Keil, T. 1997 Functional morphology of insect mechanoreceptors. *Microsc. Res. Tech.* **39**, 506–31. (doi:10.1002/(SICI)1097-0029(19971215)39:6<506::AID-JEMT5>3.0.CO;2-B)

23. Zill, S. N. & Moran, D. T. 1981 The Exoskeleton and Insect Proprioception: III. Activity of Tribal Campaniform Sensilla During Walking in the American Cockroach, Periplaneta Americana. *J. Exp. Biol.* **94**, 57–75.

24. McCullough, E. L. & Zinna, R. A. 2013 Sensilla Density Corresponds to the Regions of the Horn Most Frequently Used During Combat in the Giant Rhinoceros Beetle Trypoxylus dichotomus (Coleoptera: Scarabaeidae: Dynastinae). *Ann. Entomol. Soc. Am.* **106**, 518–523.